International Journal of the Physical Sciences Vol. 6(27), pp. 6329-6341, 2 November, 2011
Available online at http://www.academicjournals.org/IJPS
DOI: 10.5897/IJPS11.867
ISSN 1992 - 1950 ©2011 Academic Journals

Full Length Research Paper

Performance metrics for active contour models in image segmentation

Hum Yan Chai*, Teng Jih Bao, Lai Khin Wee, Tan Tian Swee and Sh-Hussain Salleh

[1]Centre for Biomedical Engineering, Faculty of Health Science and Biomedical Engineering, Universiti Teknologi Malaysia, Skudai, 81310, Johor, Malaysia.
[2]Biomedical Engineering Group, Institute of Biomedical Engineering and Informatics, Faculty of Computer Science and Automation, Technische Univeristat Ilmenau, Germany.

Accepted 28 September, 2011

Image segmentation is one of the significant techniques in image processing to distinguish desired parts from its background for further analysis. It provides visual means for inspection of anatomical structure of human body, identification of disease, tracking of its development and input for surgical planning and simulation. Active contour models are regarded as promising and vigorously research model-based approach to computer assisted medical image analysis. However, it is not trivial to assess whether one segmentation algorithm performs more superior than the other. Therefore, a systematic assessment tool is designed and implemented to examine all the important aspects of active contour models. Meanwhile, a novel supervised evaluator including analytical method and empirical methods are proposed to acts as objective evaluator. The obtained results highlighted both the strengths and limitations of the studied active contour models. A proper area usage of each active contour model is also suggested at the end of this paper.

Key words: Active contour models, assessment tool, image segmentation, objective evaluation.

INTRODUCTION

Image segmentation (Lai et al., 2011) is the process by which an image is broken into similar pieces or in which desired parts (region of interest, ROI) of an image are extracted and processed (Linda and George, 2001). It provides informative input for further image analysis. Numerous techniques incorporating artificial intelligence, such as heuristic optimization are proposed to perform the segmentation (Hao and Pu, 2011; Noor et al., 2011; Zhu et al., 2011). Its importance and application in the biomedical image processing are numerous, where it aids physicians greatly in providing visual means for inspection of anatomical human body (Worth et al, 1997), identification of disease, iris recognition which requires a fast and yet accurate iris segmentation (Zhaofeng et al., 2009), fingerprint recognition (Mehtre and Chatterjee, 1989) and tracking of disease development, such as brain tumor (Taylor, 1995). Also, it serves as input for surgical planning (Khoo et al., 1997), image-guided surgical (Grimson, 1997) and simulation (Dzung et al., 2000). However, segmentation remains a fundamental problem of computer vision (Linda and George, 2001) in low level image processing (Mirzaei et al., 2011), such as Marr-Hildreth (Mark and Alberto, 2002) and Canny edge detection (Canny, 1986); however, are not effective in locating an object of image especially medical images which usually appears in arbitrary shapes. The consideration of local information alone by these kinds of techniques could make incorrect assumptions during integration progress and subsequently would produce in-feasible object boundaries (McInerney and Terzopoulos, 1996).

In contrast, the energy minimization deformable models, such as active contour model provide a partial solution. It is invariably labeled as a promising and

*Corresponding author. E-mail: ychum2@live.utm.my.

vigorously research model-based method to computer-assisted medical image analysis (McInerney and Terzopoulos, 1996). The basic idea of active contour is allowing a contour to contort to minimize energy functional to achieve objective. These deformable models are capable of segmenting, matching and tracking images of anatomical structure (Dzung et al., 2000).

However, it is not trivial to assess whether one segmentation algorithm performs better than the other (Fenster and Chiu, 2005). Each active contour model has its own advantages and limitation. Misused of these methods would lead to the wrong medical diagnosis and redundancy in resources. Critical issues that deal with the application of active contour models in biomedical applications include the complex procedure (execution time), numerous parameter selection and sensitivity to the placement of initial contour (capture ability). Besides, to date, the popular methods to examine the effectiveness of segmentation are based on subjective evaluation method and edge detection. These current evaluators are tedious, time consuming and the applications are restricted to the edge-based active contours. Thus, in order to assess the performance of each active contour model in image segmentation, a systematic assessment tool is proposed for all important aspects. The comparative results will highlight the strengths and restrictions of the active contour models. The studied models are Kass, localized region based (LRB), level set (LS), distance snake (Distance) and Chan-Vese active contour without edges (CV).

Subsequently, typical active contour models for digital image segmentation are reviewed after which details of the designed performance evaluation are given. This is followed by establishing the result of the analysis on each active contour model in accordance with their characteristic. Finally, to illustrate the performance and properties of the active contour model, experimental results are drawn.

Medical imaging modalities

Medical imaging is a technique and process employed to produce images of the anatomical structure and physiological part of the human body (Paul, 2002). Medical imaging modalities include Ultrasound, CT scan, MRI and Nuclear Medicine PET (Dhawan, 2003; William et al., 2002; David et al., 2001; Joseph 1996, 1997, 1998, 1999, 2010; Paul, 2002). These modalities are categorized into invasive and non-invasive techniques. The invasive techniques include operation and endoscope, while non-invasive techniques comprise of modalities, such as MRI, Ultrasound, X-ray, CT and PET. All these medical imaging modalities provide different measurements enabling physicians to accomplish clinical tasks, such as patient diagnosis and monitoring more safely and effectively.

Digital image and image preprocessing techniques

A computer image is a matrix of pixels (Linda and George, 2001; Mark and Alberto, 2002; Gonzalez et al., 2004). The value of each pixel is proportional to the brightness of the corresponding point in the scene. The matrix of pixels is generally square and described as N × N m-bit pixels, where N is the number of points along the axes and m regulates the number of brightness values (Mark and Alberto, 2002). The intensity histogram shows the brightness levels of image. For 8-bit pixels, the brightness ranges from zero (black) to 255 (white). The image energy is inversely proportional to the intensity, gradient magnitude and image features.

The wiener low pass filter is deployed to degrade noise that is caused by constant power addictive (Lim and Jae, 1990). A pixel-wise adaptive Wiener method is utilized in the Wiener filter (Tachaphetpiboon and Amornraksa, 2008). The local mean and standard deviation of the each neighbor's pixel is estimated statistically.

$$\mu = \frac{1}{NM} \sum_{n_1, n_2 \in \eta} a(n_1, n_2) \quad (1)$$

$$\sigma^2 = \frac{1}{NM} \sum_{n_1, n_2 \in \eta} a^2(n_1, n_2) - \mu^2 \quad (2)$$

where η is the M by N local neighborhood of each pixel. Equation 3 shows the estimation of pixel-wise Wiener filter where v^2 denotes the noise variance.

$$b(n_1, n_2) = \mu + \frac{\sigma^2 - v^2}{\sigma^2}(a(n_1, n_2) - \mu) \quad (3)$$

Laplacian filter is one of the edge enhancement filters. It uses second derivatives information about the image intensity changes through a difference equation. It is generated by using convolution filter with a kernel (Fisher et al., 2003).

$$K = \frac{1}{4}\begin{bmatrix} 0 & -1 & 0 \\ -1 & 4 & -1 \\ 0 & -1 & 0 \end{bmatrix} \quad (4)$$

The unsharp contrast enhancement filter can be created using negative Laplacian filter by varying α value in the range of 0.1 to 1.0. The negative Laplacian filter is given as:

$$\frac{1}{(\alpha+1)}\begin{bmatrix} -\alpha & \alpha-1 & -\alpha \\ \alpha-1 & \alpha+5 & \alpha-1 \\ -\alpha & \alpha-1 & -\alpha \end{bmatrix} \quad (5)$$

Snakes and its variants

Snakes (Kass et al., 1987) or active contours are curves described inside an image domain which deform under the control of internal energy and external energy (Xu and Prince, 1998). The internal energy responsible for smoothness and stretchiness of the contour, whereas the external energy pulls the contour to the region-of-interest (ROI). The curve evolution method is deploying an energy minimization function and it can be represented as:

$$E = \int_0^1 (\alpha(s)|V_s(s)|^2 + \beta(s)|V_{ss}(s)|^2 / 2 + E_{ext}(V(s))ds \quad (6)$$

where α and β denotes weighting parameters that regulate the smoothness and stretchiness of snake, respectively. The external energy $\mathbf{E_{ext}}$ is obtained from the image which value is small at the ROI. Euler equation must be satisfied to minimize E.

$$\alpha(s)V^{'}(s) - \beta(s)V^{''}(s) - \nabla E_{ext} = 0 \quad (7)$$

Xu and Prince (1998) introduced new external forces which consist of static and dynamic forces. The gradient vector field (GVF) is described as the vector field v(x,y) = (u(x,y), v(x,y)) which minimizes the energy functional:

$$E = \iint \mu(u_x^{\ 2} + u_y^{\ 2} + v_x^{\ 2} + v_y^{\ 2}) + |\nabla f|^2 |v - \nabla f|^2 dxdy \quad (8)$$

where f denotes gray level or binary edge map, while the μ regularizes the effect of the first term in the intergrand which is a same smoothing term utilized by Horn and Schunck (1981) in their formulation of optical flow.

Li and Acton (2007) proposed another new external force which is computed by convoluting a vector field with the edge map obtained from the image. Cohen and Cohen (1993) and Lei et al. (2008) introduced another type of external function which is given as:

$$F = -\nabla Q(v) \quad (9)$$

where Q(v) denotes the minimum normalized Euclidean distance from v to an edge point with the edge point identified by a thresholded gradient. This force is formed as the negative of the external energy gradient and enables a large magnitude for the external force in the image and consequently the capture range is enlarged. The initial contour can be located far away from the desired boundary if there are no spurious edges along the way. By using a finite element method, the deform-able contour is represented as a continuous curve in the form of weighted sum of local polynomial basic functions. The result has good stability and convergence in the energy minimization process.

Li and Acton (2006) proposed a weighting function which is added into external energy to minimize the noise sensitivity of snake. Similarly, Lu and Shen (2006) uses shape similarity metric method to modify the snake in order to solve the noise problem. In this method, Fourier descriptor (Bryan, 1998, 1999, 2000; Gang et al., 2008) is an aspect for the distribution description of image pixels on image contour.

Lankton (2008) proposed a novel local region-based structure. The energy minimization is based on the investigation of each point along the curve where the energy is calculated in its local region. The curve evolution breaks the local neighborhoods into local interior and exterior and thus, computes the local energies. The smoothed Heaviside function is used for establishing the interior of closed contour. For the exterior contour, it is represented by (1- Hφ(x)).

Chunming et al. (2005) presented a new variational energy functional using level set function. It eases the costly re-initialization procedure by forcing the level set function near to a signed distance function. In the traditional methods (Vicent et al., 1997; Ravikanth et al., 1995; Osher and Fedkiw, 2003), the level set function can lead to shocks shape, while evolving the curve. The new energy functional was proposed to address the problem and is given as:

$$E(\phi) = \mu P(\phi) + E_{g,\lambda,v}(\phi) \quad (10)$$

where μP(Φ) is internal energy which penalizes the difference of Φ from sign distance function. $\mathbf{E_{g\lambda,v}}$(Φ) is external energy which consists of univariate Dirac function and Heaviside function. Chan and Vese (2001) introduced another model by taking the information within the regions into consideration not only at their edges. The segmentation problem was explicated by (Mumford and Shah, 1989) and level sets (Osher and Sethian, 1988).

Objective evaluation

Pratt (1978) brought about a figure of merit (FOM) that balances the types of errors induced by the absence of valid edge points, failure to localize edge points and classification of noise fluctuation as edge points. The equation is defined as:

$$R = \frac{I}{I_N} \sum_{i=1}^{I_A} \frac{1}{1 + ad^2} \quad (11)$$

where I_N denotes max {I_I,I_N}x and I_I and I_N entitle the number of ideal and actual edge map points, 'a' is a scaling constant and 'd' is the distance between actual

and ideal edge points. It is a normalization rating factor where R equals to unity is the perfect detected edge. Ji and Haralick (1999) proposed a novel quantitative evaluation of edge detectors by utilizing the minimum kernel variance criterion. They found out that the decision of determining a pixel as an edge is based on the outcome of the convolution of image with a kernel.

The global consistency error (GCE) which is developed by (Martin et al., 2001) acts as an objective evaluation of consistency between image segmentations. The resultant image of one algorithm is compared with respective manually segmented image to quantify the error measure. For a given pixel P_i, consider the segments S_1 and S_2 that contain P_i, the segments are sets of pixels and denoted as C(S_1, P_i) and C(S_2, P_i). Let the \ symbolize the set difference, and thus the local refinement error (LRE) and GCE are defined as:

$$LRE(S_1, S_2, P_i) = \frac{|C(S_1, P_i) \setminus C(S_2, P_i)|}{C(S_1, P_i)} \quad (12)$$

$$GCE(S_1, S_2) = \frac{1}{N} \min\left\{\sum LRE(S_1, S_2, P_i), \sum LRE(S_2, S_1, P_i)\right\} \quad (13)$$

By referring to Equation 12, if one segment is inclusive of the other, then the pixel is in the area of refinement and the LRE value is zero. The GCE forces all the local refinement to be in the same direction and thus, it assesses one segmentation can be viewed as a refinement of the other to which extent.

Meila (2005) presented Variation of Information (VoI) as a measurement of information loss and gain between the two clustering. The clusterings are viewed as elements of a lattice and its distance apart across the lattice is estimated based on mutual information metrics and entropy. In short, this nonnegative metric measures the amount of randomness in one segmentation which cannot be explained by the other. A random clustering with clusters X_1, X_2,.. X_k is entitled by a random variable X with X={1…k}, such that P_i = $|X_i|$ / n i Є X and n = $\Sigma_i X_i$ the VoI between two clustering X and Y represented as:

$$VoI(X, Y) := H(X) - 2I(X; Y) \quad (14)$$

where H(X) is representing the entropy of X and I(X,Y) is mutual information between X and Y. The lower the value of VoI denotes the greater similarity.

Probabilistic Rand Index (PRI) (Unnikrishnan et al., 2007) calculates the fraction of pixels whose labeling are consistent between the computed segmentation and the ground truth, averaging across multiple ground truth segmentations to account for scale variation in human perception. Consider a set of ground truth images {S_1, S_2, …, S_k} corresponding to an image X = {x_1, x_2, … x_N}, where a subscript indexes one of N pixels. S_{test} is the segmentation of a test image and thus, the PRI is defined as:

$$PR(S_{test}, \{S_k\}) = \frac{1}{\binom{N}{2}} \sum_{\substack{i,j \\ i<j}} \left[I(l_i^{S_{test}} = l_i^{S_{test}} p_{ij} + I(l_i^{S_{test}} \neq l_j^{S_{test}})(1 - p_{ij}) \right] \quad (15)$$

$$p_{ij} = P(l_i = l_j) = \frac{1}{k} \sum_{k=1}^{K} I(l_i^k = l_j^k) \quad (16)$$

This measure takes values in [0, 1] with maximum 1 when all the segmentations are identical.

Boundary displacement error (BDE) is proposed by Freixenet et al. (2002) to measure the average displacement error of boundary pixels between two segmented images. The distance between the pixel and the closet pixel in the other boundary image is defined as error of one boundary pixel.

MATERIALS AND METHODS

Database design

With the intent of assessing the performance of active contour models, a standard A to Z alphabet database is created. The purpose of utilizing alphabets as testing images is on account of the uniqueness and various boundary concavities patterns. It provides distinct and typical problems encountered in biomedical image segmentation. It is known that one of the two main problems associated with the utility of active contours is the convergence to the boundary concavities (Xu and Prince, 1998). The font used for alphabet database is Times New Roman with size 300 and resolution of 512 × 512.

Proposed indicator for segmentation accuracy assessment of active contour models

A novel supervised evaluator that is proposed includes analytical method and empirical methods. The equation is given as:

$$M = \frac{1}{1 + \frac{\alpha E + \beta P}{A}} \quad (17)$$

where E depicts the non-segmented area of desired ROI, P is the unwanted segmented area, A is the ideal area of ROI, α and β are the scaling factors. The default scaling factors are set at 1. The range of the indicator is [0, 1], where the 1 is the highest value for the perfectly segmented area.

α and β are the parameters used to penalize regions that are offset from the ideal region. α is used to penalize the region E, whereas β is the coefficient of P. The parameters can be relatively adjusted to indicate the significant error caused by false

Table 1. The accuracy index for each active contour model.

Alphabet	Proposed indicator value (M)				
	Kass	LRB	LS	Distance	CV
A	0.5072	0.7157	0.6977	0.6437	0.9009
B	0.4558	0.5015	0.5004	0.4777	0.9344
C	0.5314	0.8998	0.8901	0.7542	0.9235
D	0.3801	0.4379	0.4394	0.4179	0.9647
E	0.4793	0.9506	0.9180	0.7295	0.9176
F	0.5148	0.9661	0.9282	0.7458	0.9127
G	0.5288	0.9580	0.9071	0.7611	0.9512
H	0.5297	0.9867	0.9145	0.7659	0.9524
I	0.5639	0.9877	0.9523	0.7917	0.9870
J	0.5984	0.9715	0.8960	0.7763	0.9339
K	0.5299	0.9382	0.9103	0.7660	0.9398
L	0.5623	0.9705	0.9269	0.7690	0.9531
M	0.5990	0.9563	0.9121	0.7571	0.9432
N	0.6103	0.9479	0.8935	0.7406	0.9289
O	0.3426	0.3733	0.3727	0.3606	0.9432
P	0.5442	0.6559	0.6501	0.5974	0.9349
Q	0.3649	0.3949	0.3999	0.3855	0.9263
R	0.5606	0.7025	0.6901	0.6268	0.9524
S	0.6168	0.9327	0.8921	0.7558	0.9163
T	0.6289	0.9876	0.9378	0.7638	0.9884
U	0.6000	0.9691	0.9088	0.7406	0.9631
V	0.6330	0.9365	0.8963	0.7647	0.9186
W	0.6292	0.9459	0.9005	0.7638	0.9231
X	0.6316	0.9196	0.8691	0.7473	0.9248
Y	0.6329	0.9402	0.8878	0.7555	0.9253
Z	0.6299	0.9449	0.9046	0.7555	0.9466
Average	0.5460	0.8420	0.8076	0.6890	0.9387

segmentation. For example, higher value of β is deployed to emphasize the offset caused by the unwanted area. On the contrary, α is set lower than β to indicate the subordination of error. The default scaling factors are set at 1.

Image preprocessing

The preprocessing techniques, such as noise removal filter (Wiener filter) and edge enhancing filter (Laplacian filter) are used to compensate the effect of resizing of the input image. The purpose of image resizing is to accelerate the segmentation algorithm. However, it triggers the aliasing. It usually appears as "stair-step" patterns or as moiré (ripple-effect) patterns in the output image. Thus, these filters are utilized to reduce the undesired effect.

RESULTS AND DISCUSSION

Accuracy

It can be seen as shown in Table 1 that the most accuracy segmentation technique among the investigated active contour models is CV. This assessment is to evaluate the best proposed indicator value that can be achieved by each active contour model. The same experiment was executed five times for each active contour model in order to get the best score. Averagely, the CV gives the best score, 0.9387. It is also observed that the initial contour for the Kass, LRB and distance had to be placed as near as possible to the boundary of object to get the best score. In some cases, especially the LS where the number of iterations is excessive, it will lead to over segmentation. Moreover, Kass, LRB, LS and distance show the incapability to segment images that contain interior contour, such as alphabet A and B. The consistency of giving the output can be seen on the Figure 1, where CV always gives the score above 0.9 over all the alphabets.

Execution time

The average execution time of each active contour, tested with 50, 100, 150 and 200 Iterations are shown in

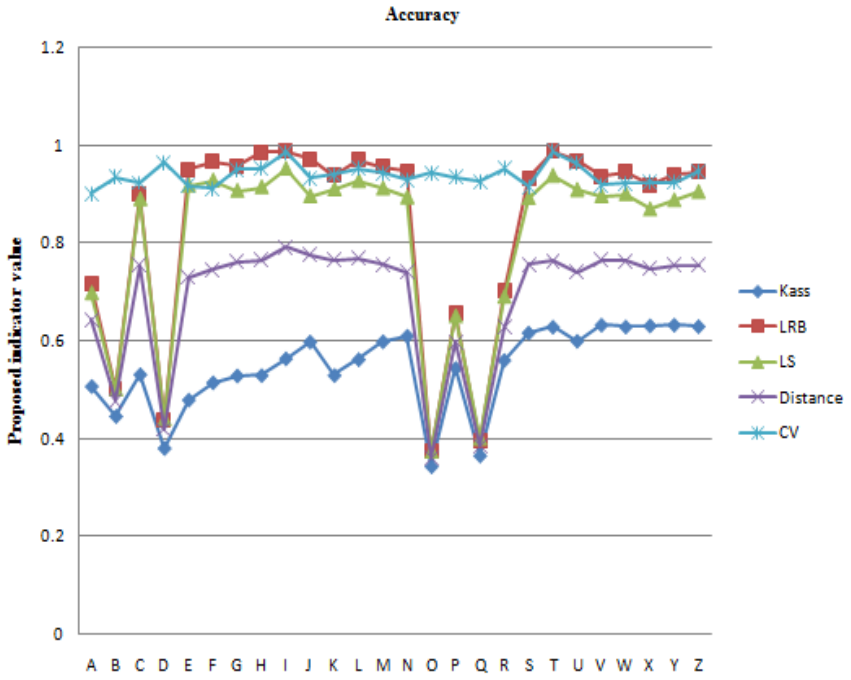

Figure 1. The segmentation accuracy of each active contour model using A to Z alphabets.

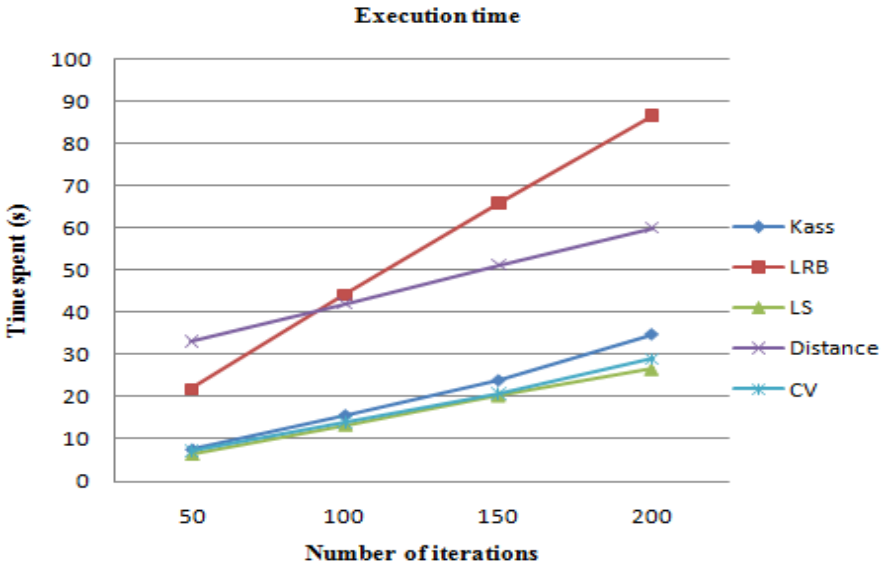

Figure 2. Average execution time of each active contour, tested with 50, 100, 150 and 200 iterations.

Figure 2. From Figure 2, it is found that the highest convergence speed of all the algorithms is the LS. The LS method implemented new variational formulation that drives the level set function approach a signed distance function. Consequently, the curve evolves without the re-initialization step. For the CV, the speed is relatively fast, because it involves no re-initialization step. By virtue of the simplicity of the Kass method which only considers the internal and external energy, the algorithm is considerably faster than the LRB and distance. The

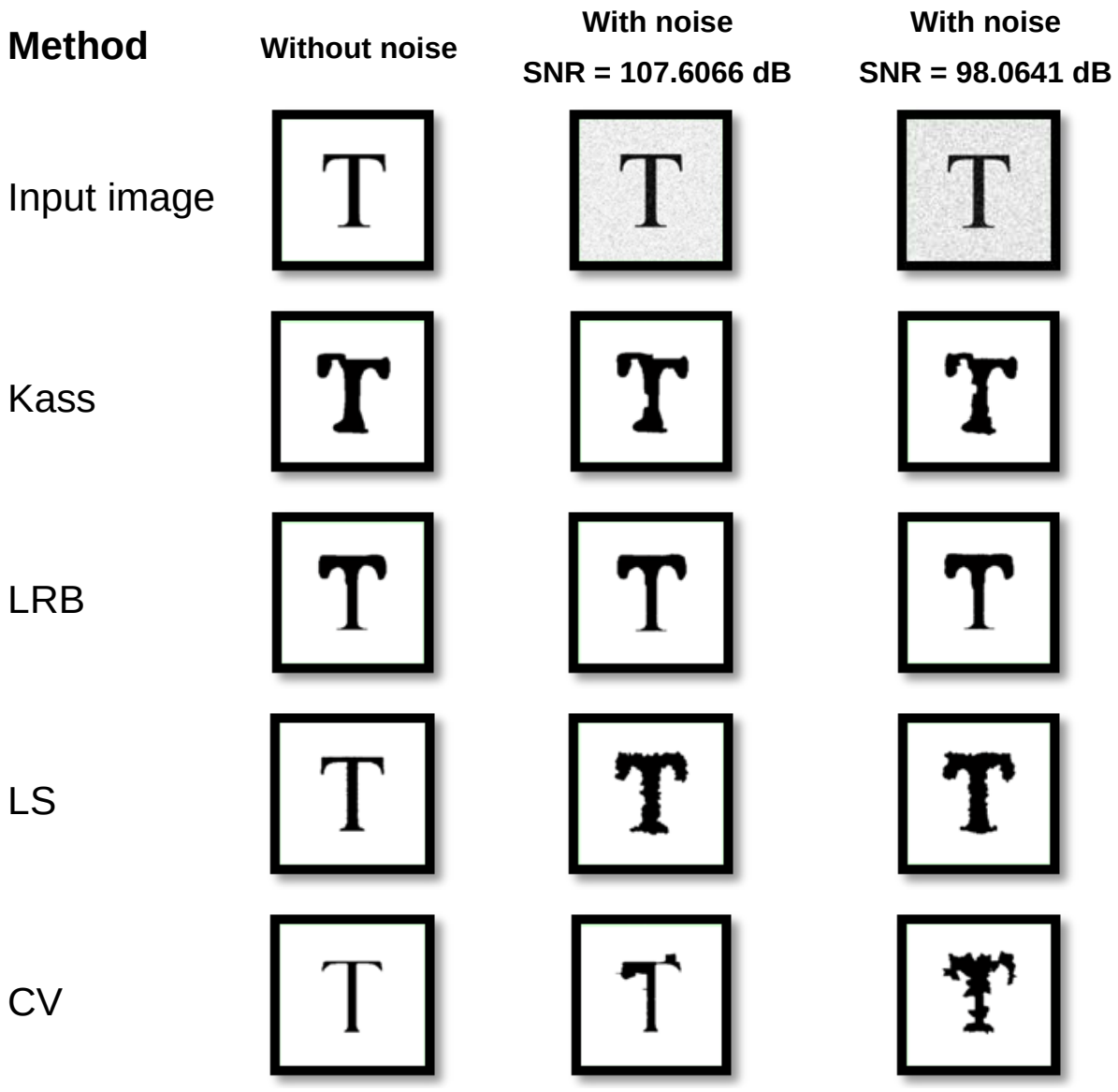

Figure 3. Illustration on the effect of imposing noise on segmentation.

subsequent step of LRB which requires re-initialization of each pixel proved costly as the time spent increases rapidly with the number of iterations. For the distance, the computation of image vector field impedes the segmentation in the initial stage. However, once the vector field is established, the contour evolves smoothly.

Noise resistance

Segmentation algorithm that possesses the high resistance to noise is favorable as the noise will distort the information in the image. The effect of the imposing noise on segmentation using the alphabet 'T' is shown in Figure 3. The result of segmentation with the existence of noise can be assessed in two techniques, by using the proposed indicator and the execution time. Based on the results from Table 2, the existence of noise in image impedes the overall segmentation performance.

The segmentation accuracy of LS has deteriorated 57.9% when compared with the result without noise. This indicates that the LS is the most sensitive to the existence of noise. On the other hand, the LRB exhibits highest resistance against the noise, which only drops 12%. Concerning the execution time, the distance computational time increases sharply by 68.7% when

Table 2. Relative error of segmentation for M, proposed indicator value and TS, time spent on images without noise and with noise.

		Without noise	With noise (SNR=107.6066 dB)	Relative error (%)	With noise (SNR=98.0641 dB)	Relative error (%)	With noise (SNR = 88.5217 dB)	Relative error (%)
Kass	M	0.4191	0.3664	12.573	0.3624	13.5347	0.3696	11.8166
	TS	15.7763	15.6284	0.9375	16.8827	7.0131	26.7342	69.458
LRB	M	0.6277	0.5520	12.0525	0.5188	17.3387	0.5069	19.2458
	TS	40.4532	40.7192	0.6575	41.7197	3.1308	42.4197	4.8612
LS	M	0.9330	0.3927	57.9147	0.3869	58.5331	0.3946	57.7079
	TS	11.0721	11.1321	0.5419	11.12	0.4326	11.1928	1.0901
Distance	M	0.7578	0.6553	13.5271	0.4275	43.5914	0.3633	52.0605
	TS	27.3575	46.1627	68.7387	76.0215	177.882	69.2804	153.24
CV	M	0.9456	0.7861	16.8662	0.7091	25.0116	0.5975	36.8089
	TS	10.6809	12.0867	13.1618	13.6526	27.5226	15.5467	45.5561

SNR, signal-to-noise-ratio.

when compare with the result without noise. As the consequence of the complexity of vector field, the overall execution time increases.

Position of initial contour

Generally, the position of initial contour gives a great impact to the final output of segmentation, especially the Kass snake. For the initialization of contour far from the object, the LRB and CV require longer time than the LS to attract the contour to the boundary. The Kass poses the weakest capture range where it is only able to segment the object that near-object initialization. Among all the studied models, only the CV is able to segment the cross-object initialization. In short, the most flexible initialization is the CV. This indicates that most of the active contour models are sensitive to the initial contour location.

Multiple objects

The ability to capture multiple objects using different active contours is illustrated in Figure 4. By visual inspection on Figure 4, the LS and CV are able to perfectly segment the multiple objects. The LRB requires many iterations and the movement of the contour is time-consuming. However, it is still possible to segment the objects. The Kass and distance shows incapability in multiple object segmentation.

Segmentation metrics

Tables 3, 4, 5 and 6 give comparative performance measure of five investigated active contour models using the three evaluation parameters. Results show that CV method gives the overall best performance with the lowest values of GCE, VoI, BDE and highest score of PRI.

Conclusion

A systematic assessment tool has been developed to assess some of the important aspects of active contour models, such as accuracy, resistance to noise, execution time consumption and multiple object segmentation ability. Furthermore, a novel supervised evaluator based on region feature is introduced. Experiment results show that the CV demonstrates better result generally among all the studied methods, followed by LRB and LS. For the evaluation on computational cost, LS has the highest algorithm

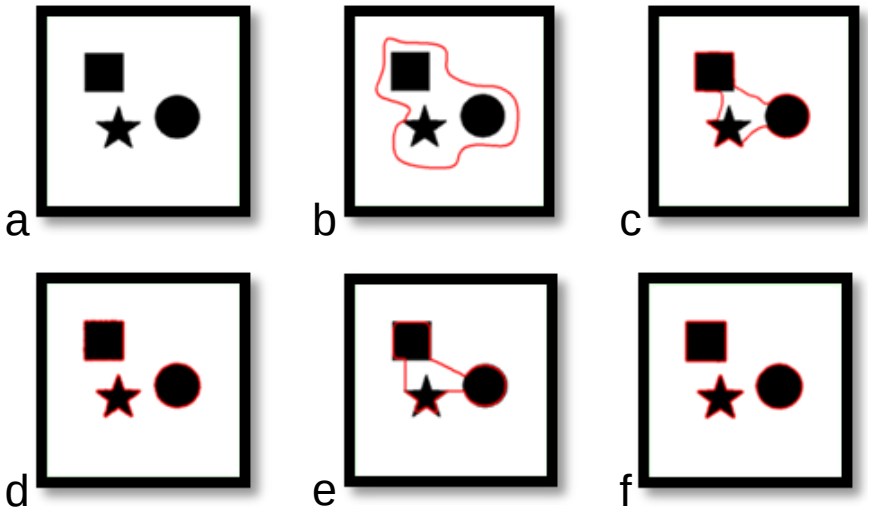

Figure 4. Ability to capture multiple objects: (a) Original image, (b) Kass, (c) LRB, (d) LS, (e) Distance and (f) CV.

Table 3. Comparison of each active contour using the GCE index (lower values indicate the better segmentation).

Alphabet	Global consistency error				
	Kass	LRB	LS	Distance	CV
A	0.0832	0.0506	0.0493	0.0680	0.0260
B	0.1320	0.1040	0.1045	0.1320	0.0271
C	0.0361	0.0271	0.0262	0.0408	0.0249
D	0.1416	0.1123	0.1126	0.1229	0.0214
E	0.0582	0.0197	0.0193	0.0449	0.0163
F	0.0406	0.0155	0.0161	0.0330	0.0141
G	0.0890	0.0259	0.0281	0.0521	0.0257
H	0.0816	0.0216	0.0218	0.0498	0.0205
I	0.0337	0.0072	0.0081	0.0229	0.0063
J	0.0345	0.0118	0.0119	0.0271	0.0109
K	0.0861	0.0254	0.0271	0.0566	0.0229
L	0.0539	0.0108	0.0119	0.0325	0.0095
M	0.0940	0.0334	0.0361	0.0727	0.0315
N	0.0687	0.0237	0.0251	0.0492	0.0223
O	0.1330	0.1174	0.1178	0.1246	0.0299
P	0.0848	0.0559	0.0560	0.0698	0.0186
Q	0.1498	0.1305	0.1297	0.1390	0.0353
R	0.1126	0.0660	0.0671	0.0875	0.0224
S	0.0758	0.0266	0.0281	0.0447	0.0262
T	0.0526	0.0094	0.0105	0.0343	0.0085
U	0.0640	0.0183	0.0205	0.0459	0.0174
V	0.0641	0.0248	0.0263	0.0409	0.0247
W	0.0894	0.0412	0.0441	0.0675	0.0405
X	0.0894	0.0352	0.0364	0.0537	0.0336
Y	0.0588	0.0235	0.0234	0.0395	0.0230
Z	0.0737	0.0255	0.0265	0.0478	0.0242
Average	0.0800	0.04090	0.0417	0.0615	0.0225

Table 4. Comparison of each active contour using the VoI index (lower values indicate the better segmentation).

Alphabet	Variation of information				
	Kass	LRB	LS	Distance	CV
A	0.6361	0.4507	0.4410	0.5318	0.3002
B	0.9824	0.7713	0.7807	0.9824	0.3105
C	0.4508	0.2807	0.2863	0.3778	0.2754
D	1.0600	0.8755	0.8992	0.9876	0.2546
E	0.5253	0.2276	0.2786	0.3652	0.2175
F	0.4030	0.1765	0.2339	0.2883	0.1988
G	0.6788	0.2852	0.3244	0.4440	0.2916
H	0.6304	0.2211	0.3083	0.3834	0.2694
I	0.2796	0.1070	0.1358	0.1866	0.0984
J	0.3173	0.1628	0.1438	0.2302	0.1282
K	0.6733	0.2975	0.3375	0.4559	0.2778
L	0.4100	0.1587	0.1883	0.2597	0.1461
M	0.8111	0.3739	0.4523	0.5819	0.3628
N	0.6126	0.2578	0.3430	0.4228	0.2786
O	1.1263	0.9690	0.9808	1.0491	0.3163
P	0.6515	0.4439	0.4534	0.5424	0.2082
Q	1.2212	1.0394	1.0483	1.1210	0.3671
R	0.7870	0.5415	0.5686	0.6698	0.2725
S	0.6127	0.2817	0.3135	0.4030	0.2878
T	0.4227	0.1483	0.1976	0.2683	0.1462
U	0.5404	0.2373	0.2702	0.3796	0.2299
V	0.5400	0.2806	0.2971	0.3747	0.2771
W	0.7973	0.4314	0.4771	0.5952	0.4436
X	0.7099	0.3508	0.3858	0.4775	0.3426
Y	0.5058	0.2582	0.2734	0.3537	0.2746
Z	0.6093	0.2867	0.3154	0.4013	0.2787
Average	0.6536	0.3813	0.4129	0.5051	0.2636

Table 5. Comparison of each active contour using the BDE index (lower values indicate the better segmentation).

Alphabet	Boundary displacement error				
	Kass	LRB	LS	Distance	CV
A	5.2050	2.4750	2.3227	3.1545	0.3813
B	7.3943	6.7691	6.4258	7.3943	0.5357
C	13.0452	0.4727	0.4169	1.5106	0.3387
D	7.5810	5.4015	5.3833	5.4974	0.4448
E	6.8450	0.9238	0.8991	2.7770	0.5346
F	8.3042	0.8143	0.7633	3.7226	0.5150
G	4.3079	0.3780	0.5529	1.5455	0.3467
H	6.5166	0.6484	0.8144	3.8511	0.6324
I	5.8261	0.7785	0.7951	3.9335	0.6418
J	5.8962	0.5923	0.7334	3.0726	0.7065
K	4.0202	0.6696	0.5348	2.1084	0.4919
L	4.2095	0.9159	0.8594	3.2148	0.6056
M	5.2942	0.6221	0.8252	1.9795	0.4149

Table 5. Cont'd

N	4.7154	0.4544	0.7676	1.9903	0.4722
O	5.9653	5.0169	5.0608	4.8021	0.3948
P	5.9701	3.7958	3.7719	4.3853	0.3580
Q	5.8594	4.4666	4.2298	4.3449	0.3625
R	5.2747	2.6574	2.7302	3.5213	0.4199
S	3.7471	0.3998	0.4877	1.5968	0.3515
T	5.1244	0.9101	0.7304	3.2562	0.7095
U	4.0962	0.5604	0.8773	2.3922	0.4777
V	2.9346	0.2967	0.3300	1.5401	0.3114
W	3.4300	0.3767	0.4406	1.6403	0.3307
X	2.7984	0.5503	0.4526	1.4778	0.4641
Y	3.3629	0.4932	0.5384	2.1300	0.4451
Z	3.4881	0.4897	0.4904	1.5129	0.4159
Average	5.4312	1.6127	1.6244	3.0135	0.4655

Table 6. Comparison of each active contour using the PRI index (higher values indicate the better segmentation).

Alphabet	Variation of information				
	Kass	**LRB**	**LS**	**Distance**	**CV**
A	0.9075	0.9453	0.9469	0.9311	0.9751
B	0.8017	0.8369	0.8364	0.8017	0.9763
C	0.9221	0.9781	0.9783	0.9579	0.9795
D	0.7557	0.7936	0.7919	0.7810	0.9823
E	0.9095	0.9811	0.9769	0.9490	0.9827
F	0.9273	0.9844	0.9802	0.9547	0.9837
G	0.9046	0.9796	0.9751	0.9512	0.9789
H	0.8967	0.9808	0.9728	0.9421	0.9771
I	0.9600	0.9907	0.9886	0.9752	0.9918
J	0.9540	0.9843	0.9883	0.9703	0.9892
K	0.9051	0.9758	0.9722	0.9483	0.9774
L	0.9430	0.9859	0.9831	0.9663	0.9869
M	0.8679	0.9707	0.9615	0.9320	0.9725
N	0.9030	0.9791	0.9684	0.9447	0.9765
O	0.7396	0.7644	0.7639	0.7570	0.9759
P	0.8923	0.9307	0.9288	0.9170	0.9838
Q	0.7307	0.7601	0.7604	0.7523	0.9731
R	0.8708	0.9224	0.9195	0.9018	0.9803
S	0.9197	0.9798	0.9767	0.9567	0.9795
T	0.9342	0.9858	0.9824	0.9633	0.9869
U	0.9292	0.9814	0.9783	0.9531	0.9831
V	0.9333	0.9782	0.9766	0.9608	0.9788
W	0.8901	0.9668	0.9620	0.9347	0.9650
X	0.9116	0.9732	0.9701	0.9492	0.9747
Y	0.9331	0.9796	0.9780	0.9596	0.9781
Z	0.9175	0.9781	0.9757	0.9560	0.9789
Average	0.8908	0.9449	0.9420	0.9218	0.9795

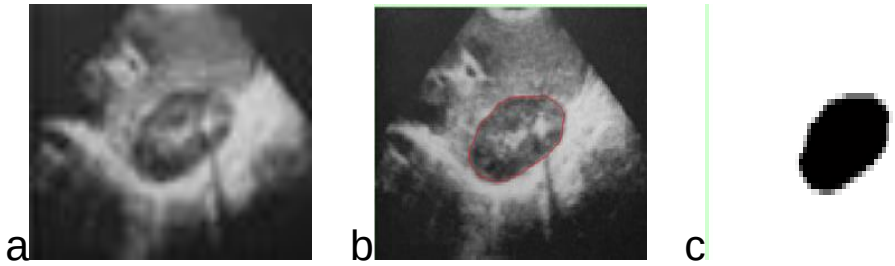

Figure 5. Application of active contour model in medical image (a) input noisy ultrasound image, (b) segmentation using LRB and (c) output image.

speed. On contrary, the LRB posed the highest computational cost. However, this method has the most robustness towards noise. In general, the decision of placing initial contour has great impact to the final segmentation results. Contour which is initialized near to the edge of ROI will get the best result. The most flexible initialization is the CV. It shows the capability of segment object(s) regardless of the distance of initial contour. The results from segmentation metrics also show that CV gave the minimal boundary error and highest consistency among all the investigated models.

Based on all the experiments that had been carried out, it is suggested that the LRB is best suited for analyzing the ultrasound image. Its high robustness to the noise and considerably high accuracy make it the most appropriate method to examine the noisy image. For the MRI images, particularly those that entail the scanning of brain, the CV is the most suitable in consideration of its high accuracy.

The future research will focus on analyzing more properties of active contour model in image segmentation and exploring the influences of each property in different environment. Besides, the significance and intuition of each property in different application would be investigated in order to optimize the performance of segmentation in different application in future research.

RECOMMENDATION

Based on the results and discussion, a few recommendations can be drawn out for the area usage of studied active contour models in medical images. For the noisy ultrasound medical imaging, it is recommended that the LRB is the most suitable segmentation method due to its high noise resistance. Figure 5 shows the application of LRB in a noisy ultrasound image. The initialization of contour was placed near to the tumor (ROI) and number of iteration was set at 100. Results show that it was able to crop the kidney accurately. Active contour models, while serving as segmentation tools in medical image diagnosis has been selected by considering their properties. Different method will give distinct output. LRB poses the local segmentation by extracting the tumor alone, whereas the CV is global segmentation. The CV method is a powerful segmentation tool that could perform global anatomical structure segmentation.

REFERENCES

Bryan S (1998-2000). Morse. Shape Description (Contours). Brigham Young University, pp. 34-50.

Canny J (1986). A computational approach to edge detection. IEEE Trans. Pattern Analysis and Machine Intelligence, 8(6): 679-698.

Chan T, Vese L (2001). Active contours without edges. IEEE Trans. Image Process, 10: 266-277.

Chunming L, Xu C, Gui C, MD Fox (2005). Level set evolution without re-initialization: A new variational formulation, San Diego, CA.

Cohen L, Cohen I (1993). Finite element methods for active contour models and balloons for 2-D and 3-D images, IEEE Trans. Pattern Anal. Machine Intell. 15(11):1131-1147.

David JB, Carl DE, Eric JH, Walter EB (2001). Estimated risks of radiation-induced fatal cancer from pediatric CT. Am J. Roentgenology 176: 289-296.

Dhawan PA (2003). Medical imaging analysis. NJ: Wiley Interscience Publication, pp. 67-90.

Dzung LP, Chenyang X, Jerry LP (2000). Current methods in medical image segmentation. Ann. Rev. Biomed. Eng., 2:315-337.

Fenster A Chiu B (2005). Evaluation of segmentation algorithms for medical imaging. Annual International Conference of the IEEE Engineering in Medicine and Biology - Proc 7 VOLS, art. no. 1616166, pp. 7186-7189.

Fisher R, Perkins S, Walker A, Wolfart E (2003). Spatial Filters-Laplacian of Gaussian. http://homepages.inf.ed.ac.uk/rbf/HIPR2/log.htm.

Freixenet J, Muñoz X, Raba D, Martí J, Cufí X (2002). Yet Another Survey on Image. Springer, 47: 7–42. doi: 10.1023/A: 1014573219977.

Gang Z, Ma ZM, Qiang T, Ying H, Tienan Z (2008). Shape feature extraction using fourier descriptors with brightness in vontent-Based medical image retrieval. International Conference on Intelligent Information Hiding and Multimedia Signal Processing, pp. 71 - 74.

Grimson WEL, Ettinger GJ, Kapur T, Leventon ME, Wells WM, Kikinis R (1997).Utilizing segmented MRI data in image-guided surgery. Int. J. Patt. Rec. Art. Intel., 11:1367-1397.

Hao X, Pu W (2011). An improved genetic algorithm for solving simulation optimization problems. Int J. Phys. Sci. 6(10): 2399-2404.

Horn BKP, Schunck BG (1981). Determining optical flow. Artif. Intell., 17:185-203.
Ji Q, Haralick RM (1999). Quantitative evaluation of edge detectors using the minimum kernel variance criterion. In Proceedings of ICIP (2):705-709
Joseph PH (1996-2010). The Basics of MRI, E-Book, pp. 23-80.
Kass M, Witkin A, Terzopoulos D (1987). Snakes - active contour models. Int. J. Comput. Vision, 1: 321-331.
Khoo VS, Dearnaley DP, Finnigan DJ, Padhani A, Tanner SF, Leach MO (1997). Magnetic resonance imaging (MRI): considerations and applications in radiotheraphy treatment planning. Radiother, Oncol., 42:1-15.
Lai Khin Wee, Hum Yan Chai, Eko Supriyanto (2011). Three dimensional nuchal translucency ultrasound segmentation using region growing for trisomy 21 early assessment. Int. J. Phys. Sci., 6(15):3704-3710.
Lankton S (2008). Localizing region-based active contours. IEEE Transactions On Image Processing, 17: 2029 - 2039.
Lei H, Zhigang P, Bryan E, Xun W, Chia YH, Kenneth LW, William GW (2008). A comparative study of deformable contour methods on medical image segmentation. Image and Vision Computing, 26:141-163.
Li B, Acton ST (2006). Feature Weighted Active Contours for Image Segmentation. Proceedings of IEEE Southwest Symposium on Image Analysis and Interpretation, pp. 188 - 192.
Li B, Acton ST (2007). Vector field convolution for image segmentation using snakes. IEEE Int. Conf. Image Processing, Atlanta, GA.
Li B, Acton ST (2007). Vector field convolution for image segmentation using snakes. IEEE Trans. On Image Processing, 16: 1637-1640.
Lim, Jae S (1990). Two dimensional signal and image processing. Englewood Cliffs, NJ, Prentice Hall, pp. 548-550.
Linda G Shapiro, George C Stockman (2001). Computer vision. New Jersey, Prentice-Hall, pp. 279-325.
Lu R, Shen Y (2006). Noisy Image Segmentation by Modified Snake Model. J. Phys. Conf. Ser. *48*:369-372.
Mark SN, Alberto S Aguado (2002). Feature extraction and image processing. Reed Educational and Professional Publishing Ltd, pp. 45-60.
Martin D, Fowlkes C, Tal D, Malik J (2001). A database of human segmented natural images and its application to evaluating segmentation algorithms and measuring ecological statistics. Proc. IEEE Int. Conf. Comput. Vision, 2: 416–423, ISBN: 0-7695-1143-0, Vancouver, July 2001.
McInerney T, Terzopoulos D (1996). Deformable models in medical image analysis: A survey. Medical Image Analysis. 1(2):91-108.
Mehtre BM, Chatterjee B (1989). Segmentation of fingerprint images -- A composite method. Pattern Recognition 22(4): 381-385.
Meilă M (2005). Comparing clusterings - An axiomatic view, Proceedings of the 22nd international conference on Machine learning, pp. 577-584.
Mirzaei K, Motameni H, Enayatifar R (2011). New method for edge detection and de noising via fuzzy cellular automata. Int. J. Phys. Sci., 6(13): 3175-3180.
Mumford D, Shah J (1989). Optimal approximation by piecewise smooth functions and associated variational problems. Commun. Pure Appl. Math, 42:577-685.
Noor MM, Kadirgama K, Rahman MM (2011). Particle swarm optimisation prediction model for surface roughness. Int. J. Phys. Sci. 6(13): 3082-3090.
Osher S, Fedkiw R (2003). Level Set Methods and Dynamic Implicit Surfaces, New York: Cambridge Univ. Press, pp. 50-60.
Osher S, Sethian JA (1988). Fronts propagating with curvature-dependent speed: Algorithms based on Hamilton-Jacobi Formulation. J. Comput. Phys., 79:12-49.
Paul S (2002). Fundamentals of medical imaging, Cambridge University Press, pp. 60-90.
Pratt WK (1978). Digital Image Processing, Wiley, New York, pp. 55-70.
Gonzalez RC, Woods RE Eddins SL (2004). Digital image processing using MATLAB, Pearson Education, Inc, pp. 70-90.
Ravikanth M, James AS, Baba CV (1995). Shape modeling with front propagation: A level set approach. IEEE Trans. Patt. Anal. Mach. Intell., 17:158-175.
Tachaphetpiboon S, Amornraksa T (2008). The Pixel-wise adaptive wiener filter watermarking. International Symposium on Intelligent Signal, Processing and Communication Systems Swissôtel Le Concorde, Thailand, pp. 1-4.
Taylor P (1995). Invited review: computer aids for decision-making in diagnostic radiology- a literature review. Brit. J. Radiol., 68:945-957.
Unnikrishnan R, Pantofaru C, Hebert M (2007). Toward objective evaluation of image segmentation algorithms. IEEE Trans. Patt. Anal. Mach. Intell., 29(6): 929-944.
Vicent C, Ron K, Guillermo S (1997). Geodesic active contours. Int. J. Comp. Vis., 22:61-79.
William R Hendee, Russell Ritenour E (2002). Medical imaging physics, John Wiley & Sons, Inc, pp. 45-60.
Worth AJ, Makris N, Caviness VS, Kennedy DN (1997). Neuroanatomical segmentation in MRI: technological objectives. Int. J. Patt. Rec. Art. Intel., 11:1161-1187.
Xu CY, Prince JL (1998). Snakes, shapes, and gradient vector flow. IEEE Trans. Image Proces., 7: 359-369.
Zhaofeng H, Tieniu T, Zhenan S, Xianchao Q (2009). Toward accurate and fast iris segmentation for iris biometrics. Pattern Analysis and Machine Intelligence, IEEE Transactions on, 31(9):1670-1684.
Zhu Z, Liu P, Zheng Y, Zhao J, Li S, Wang J (2011). Hybrid filtering model based on particle swarm optimization and genetic algorithm. Int. J. Phys. Sci., 6(14): 3518-3523.